Numerical Simulation of Droplet Breakup when Impacting a Narrow Gap

M. Andredaki[1], D. J. Bouchard[2], A. Georgoulas*[1], S. Chandra[2], M. Marengo[1]
[1]Advanced Engineering Centre, School of Computing Engineering and Mathematics, University of Brighton, Brighton, U.K.
[2]Department of Mechanical and Industrial Engineering, University of Toronto, Toronto, Canada
*Corresponding author: A.Georgoulas@brighton.ac.uk

Abstract
When a droplet impacts a pore with sufficiently high velocity the droplet breakups into liquid patterns both above the surface and inside the pore. In the present work, Computational Fluid Dynamics (CFD) simulations are carried out, considering the results obtained by an experimental analysis of droplets impacting on a single narrow gap, to study the factors that control the resulting droplet breakup. The single pore has the form of a slit with a width of either 100 or 150 microns across, and is several times longer than the impacting drop diameter. A droplet with a diameter of 2 mm impacts the gap at either 0.5 or 1.5 m/s. Both the experiments and the numerical simulations show that the droplet remains intact at 0.5 m/s but on the contrary cleaves into two halves at 1.5 m/s. A VOF-based numerical simulation framework that has been previously implemented in OpenFOAM and has been validated against droplet impacts on surfaces with different wettabilities, is utilised to reproduce these experimental runs. Experimental measurements are unable to capture the pressure and velocity fields that develop within the drop at the various stages of impact, however detailed pressure and velocity fields are predicted by the numerical simulation. From the overall analysis of the numerical predictions, characteristic pressure gradients within the droplet are revealed. Furthermore, the volume of the droplet that penetrates into the gaps with respect to time is quantified in detail utilising the numerical simulation results, revealing that the impact velocity does not significantly affect the early stages of the droplet penetration into the considered narrow gaps, while the gap width has a considerable effect in the droplet penetration rate from the early stages of the considered droplet impacts.

Keywords
VOF Modelling, Droplet Cleaving, Narrow Gaps, Pressure distribution, break up characteristics

Introduction

Micro-scale fluid flow phenomena are involved in a variety of applications and research areas [1]. The deep understanding of the behaviour of droplets that impact and spread on porous surfaces is important for a variety of industrial applications, such as ink-jet printing, impact of raindrops on textiles, spray painting on wooden surfaces and concrete walls, 3D-printing, needle-less delivery of drugs through human skin, irrigation etc. Droplet spreading on solid flat surfaces has been the subject of numerous experimental and numerical studies over the last few decades (e.g. [2–4]). However, droplet impact on porous media is still far from being fully understood. Studies of such micro-scale fluid phenomena need careful and combined consideration of droplet dynamics and porous media characteristics. Generally, this phenomenon is controlled by two main counter-acting processes: droplet spreading on porous surfaces and imbibition inside the porous media [5]. As the droplet spreads on the surface it also fills the voids of the porous material mainly due to capillary action. The spreading behaviour of the impinging droplet on the surface is known to depend on the liquid properties, i.e. density, viscosity and surface tension as well as on the impact conditions such as the initial droplet size, impact velocity, and surface wettability [6]. Absorption, on the other hand, is governed by both, the liquid and the porous medium properties, like porosity, pore size and pore wettability [7]. Most of the previously mentioned porous surfaces, that droplets interact with (e.g. paper, textiles, soil), are usually opaque and this makes it difficult to observe and study their interaction with impacting droplets. Furthermore, most impacting droplets will spread to their maximum diameter in the order of a few milliseconds. The temporal resolution of non-destructive scanning techniques that could be applied to study the penetration of droplets in such porous surfaces is well above this timescale. Therefore, the amount of liquid that is absorbed into a porous media during droplet impact and spreading, cannot be quantified in detail in order to explore how this influences the dynamics of the droplet impact phenomenon.

Previous experimental investigations (e.g. [8–11]) highlighted the need for experimental measurements that can simultaneously visualise the droplet above and below a surface during impact, in order to understand the role that the pore size has on the droplet spreading. Such controlled experiments have recently reported in [12], where the

influence of a long narrow pore, created by two closely spaced glass plates, on the droplet impact characteristics, is studied. In the present work, high-resolution, 3D, transient, CFD-based numerical simulations are carried out, reproducing four of the proposed experimental runs. The considered single pore has the form of a slit with either 100 or 150 microns across and is several times longer than the diameter of the drop. A droplet with a diameter of 2 mm impacts the gap at 0.5 or 1.5 m/s. An enhanced VOF-based numerical simulation framework that has been previously implemented in OpenFOAM and validated against droplet impacts on surfaces with different wettabilities is utilised to reproduce these experimental runs [13] [14]. The proposed model enhancements include a special treatment for the reduction of spurious velocities in the vicinity of the liquid-gas interface as well as the implementation of an enhanced dynamic contact angle treatment to accurately account for the wettability of the impact surfaces [15].

Numerical Method

With the VOF approach, the transport equation for the volume fraction, α, of the secondary (dispersed) phase is solved simultaneously with a single set of continuity and Navier–Stokes equations for the whole flow field. The corresponding volume fraction of the primary phase is simply calculated as $(1-\alpha)$. The main underlying assumptions are that the two fluids are Newtonian, incompressible, and immiscible. The governing equations can be written as:

$$\nabla \cdot \vec{U} = 0 \tag{2}$$

$$\frac{\partial \rho_b \vec{U}}{\partial t} + \nabla \cdot \left(\rho_b \vec{U}\vec{U}\right) = -\nabla p + \nabla \cdot \mu_b \left(\nabla \vec{U} + \nabla U^T\right) + \rho_b f + F_s \tag{3}$$

$$\frac{\partial a}{\partial t} + \nabla \cdot \left(\alpha \vec{U}\right) - \nabla \cdot (\alpha(1-\alpha)U_r) = 0 \tag{4}$$

where $\vec{U}$ is the fluid velocity vector ρ_b and μ_b are the bulk fluid density and the bulk dynamic viscosity that are calculated as weighted averages of the liquid (ρ, μ) and gaseous ($\hat{\rho}$, $\hat{\mu}$) phase properties as follows,

$$\rho_b = \rho\alpha + \hat{\rho}(1-\alpha) \tag{5}$$

$$\mu_b = \mu\alpha + \hat{\mu} + \hat{\mu}(1-\alpha) \tag{6}$$

The surface tension force F_s is modelled as a volumetric force using the Continuum Surface Force (CSF) method by Brackbill et al. [16], applying the following equations:

$$F_s = \gamma \kappa (\nabla \alpha) \tag{8}$$

$$\kappa = \nabla \cdot \left(\frac{\nabla \tilde{\alpha}}{|\nabla \tilde{\alpha}|}\right) \tag{9}$$

where γ is the surface tension coefficient and κ is the curvature of the interface. As mentioned in the introduction section of the present paper the utilized numerical framework constitutes an enhanced version of the original VOF-based solver of OpenFOAM [13], that suppresses numerical artefacts of the original model, known as “spurious currents”. The proposed enhancement involves the calculation of the interface curvature κ using the smoothed volume fraction values $\tilde{\alpha}$, which are obtained from the initially calculated α field, smoothing it over a finite region near the interface. All other equations are using the initially calculated (non-smoothed) volume fraction values of α. As mentioned previously Kistler’s model [15] has been also implemented in the proposed VOF solver which calculates the DCA, θ_d, using the Hoffman function, f_{Hoff}, as follows:

$$\theta_d = f_{Hoff}\left[C_a + f_{Hoff}^{-1}(\theta_\varepsilon)\right] \tag{10}$$

where θ_ϵ is the equilibrium contact angle. The capillary number, C_a, is calculated as $C_a = \frac{\mu U_{CL}}{\gamma}$ and U_{CL}, is the spreading velocity of the contact line. f_{Hoff}^{-1} is the inverse function of “Hoffman’s” empirical function which is calculated as shown below.

$$f_{Hoff} = acos\left[1 - 2tanh\left(5.16\left(\frac{x}{1+1.31x^{0.99}}\right)^{0.706}\right)\right] \tag{11}$$

Further details on the development and validation of the proposed numerical modelling framework can be found in [13] and [14].

Application of Numerical Method

As mentioned previously in the present work four specific cases from the droplet impact experiments reported in [12], are numerically reproduced. For this purpose, the previously described numerical simulation framework is utilised for the conduction of high-resolution, 3D, transient numerical simulations, aiming firstly to an additional validation study and secondly to give quantitative information that are difficult to be obtained from the post-processing and analysis of the experimental measurements. A schematic representation of the investigated phenomenon and the considered initial conditions are depicted in Figure 1. As it can be observed a 2mm diameter water droplet at ambient conditions impacts at a narrow gap that has a width of either 100 or 150 μm, with an impact velocity of either 0.5 or 1.5 m/s. The horizontal surfaces to the left and right side of the narrow gap, where the spreading of the droplet takes place after the impact, have a wettability that is characterised by an advancing and a receding contact angle of 92.8° and 27.0°, respectively. The vertical surfaces between which the imbibition of the droplet takes place are characterised by an advancing and a receding contact angle of 36.6° and 8.2°, respectively.

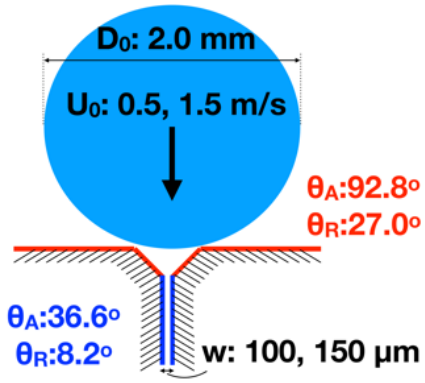

Figure 1. Schematic representation and initial conditions of investigated phenomenon

The main initial conditions, the geometric characteristics and the computational grid size for the proposed numerical simulations are summarised in Table 1, while the utilised computational geometry, mesh and boundary conditions are depicted in Figure 2.

Table 1. Initial conditions, geometric characteristics and computational grid size of numerically reproduced droplet impact cases

	D_0 [mm]	U_0 [m/s]	w [μm]	No. of Cells
Case 1	2.0	0.5	100	61,418,900
Case 2	2.0	1.5	100	61,418,900
Case 3	2.0	0.5	150	61,500,767
Case 4	2.0	1.5	150	61,500,767

As it can be observed a 3D, uniform, structured mesh with two successive levels of local grid refinement in the regions of droplet spreading and imbibition is used in each case. The overall size of the computational meshes is 61,418,900 and 61,500,767 cells for the geometries with the 100 μm and 150 μm gap, respectively. A total of 5 ms after the droplet impact were simulated for each case utilising parallel calculations with 600 computational cores in a High-Performance-Computing (HPC) facility, however only times up to 1.5 ms that the droplet spreading is within the square central region with smallest cells (second level of cell refinement) are considered, since the accuracy of the phenomenon deteriorates when the droplet goes beyond of this fine mesh domain. A later time greater than 3.00 ms is only used to indicate whether or not the droplet impact has resulted in an intact or cleaved droplet. The high number of computational cells is generally needed, in order to adequately capture the imbibition profiles within the narrow gaps.

A comparison of the experimental high-speed images with the corresponding numerically predicted snapshots of the water/air interface evolution, is conducted in Figures 3, 4, 5 and 6, for Cases 1, 2, 3 and 4, respectively. In each case the corresponding distribution of the numerically predicted velocity and relative pressure fields is illustrated in a central section plane, that passes from the middle of the narrow gap. Finally, a top view of the droplet surface evolution coloured by the velocity magnitude is shown for a later stage after the impact, for each case.

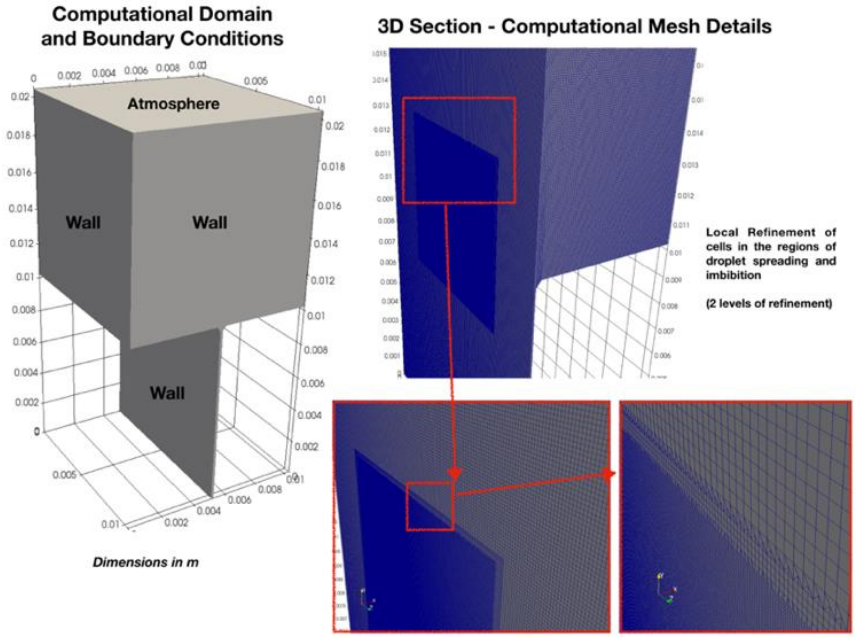

Figure 2. Computational geometry, mesh and boundary conditions.

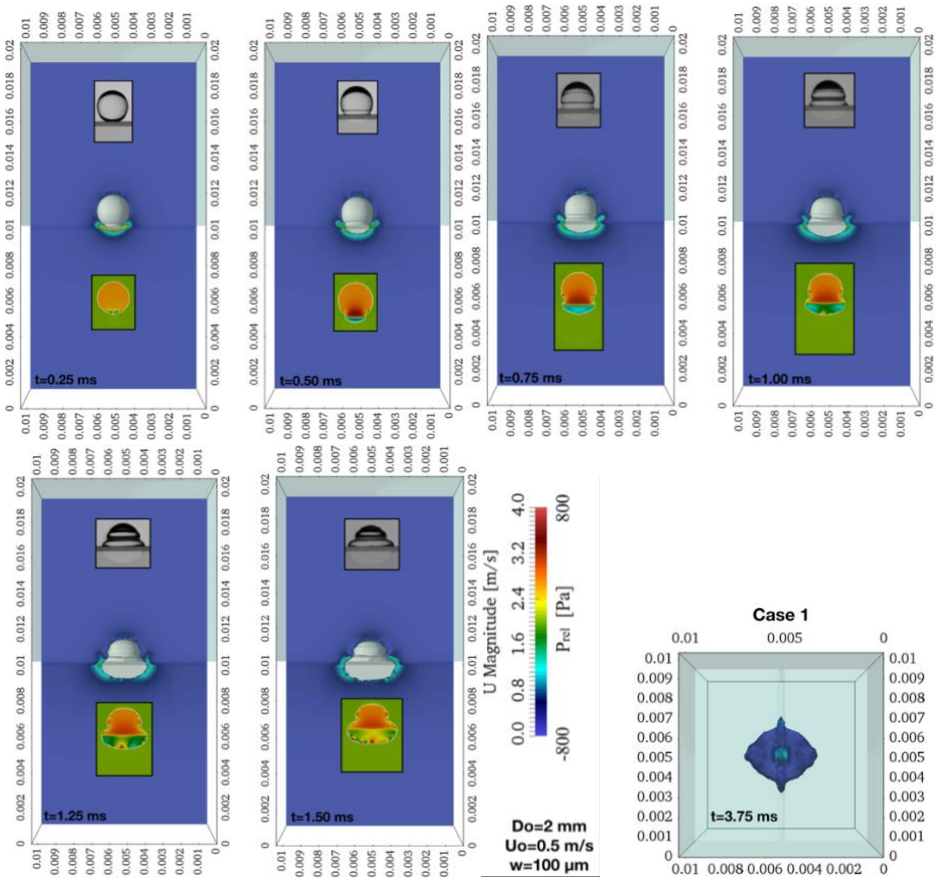

Figure 3. Droplet evolution with time for Case 1 (Table 1). Each time instance up to t = 1.50 ms illustrates the experimental snapshots from [12] (top), the numerically predicted droplet interface with a central section of the predicted velocity distribution (middle/main image) and a central section pressure distribution (bottom). For time t=3.75 ms the top view of the droplet surface is depicted, coloured by the velocity magnitude.

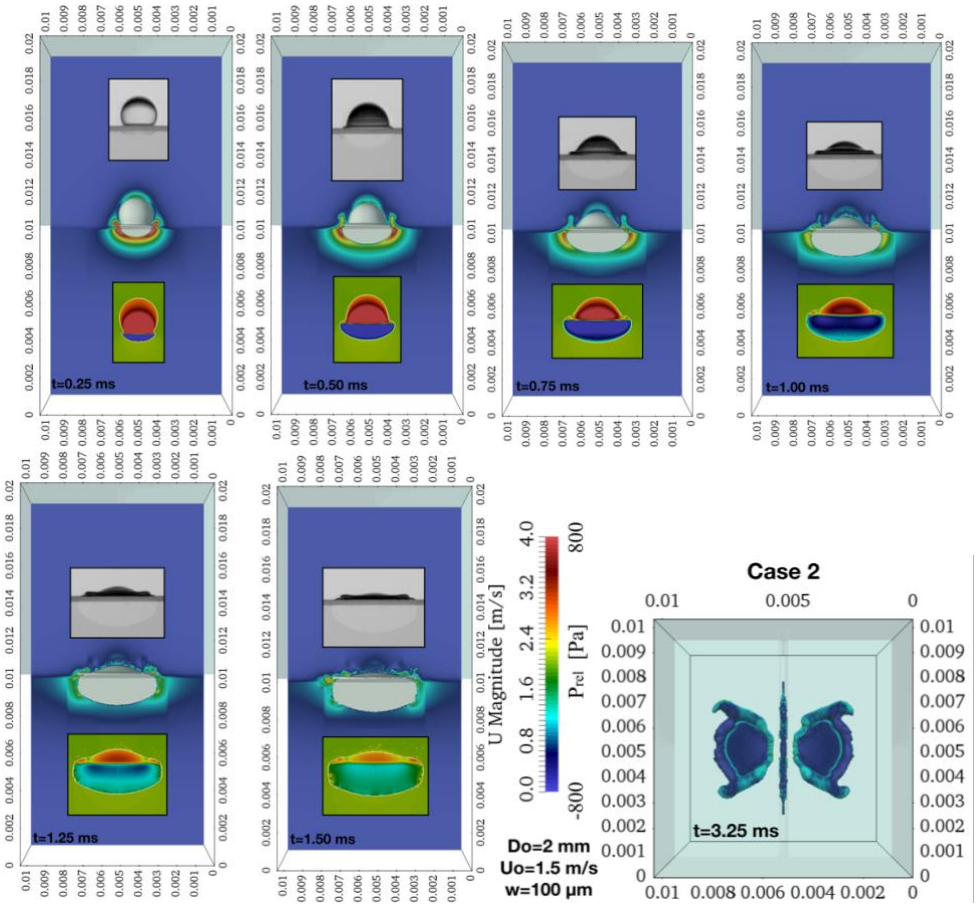

Figure 4. Droplet evolution with time for Case 2 (Table 1). Each time instance up to t = 1.50 ms illustrates the experimental snapshots from [12] (top), the numerically predicted droplet interface with a central section of the predicted velocity distribution (middle/main image) and a central section pressure distribution (bottom). For time t=3.25 ms the top view of the droplet surface is depicted, coloured by the velocity magnitude.

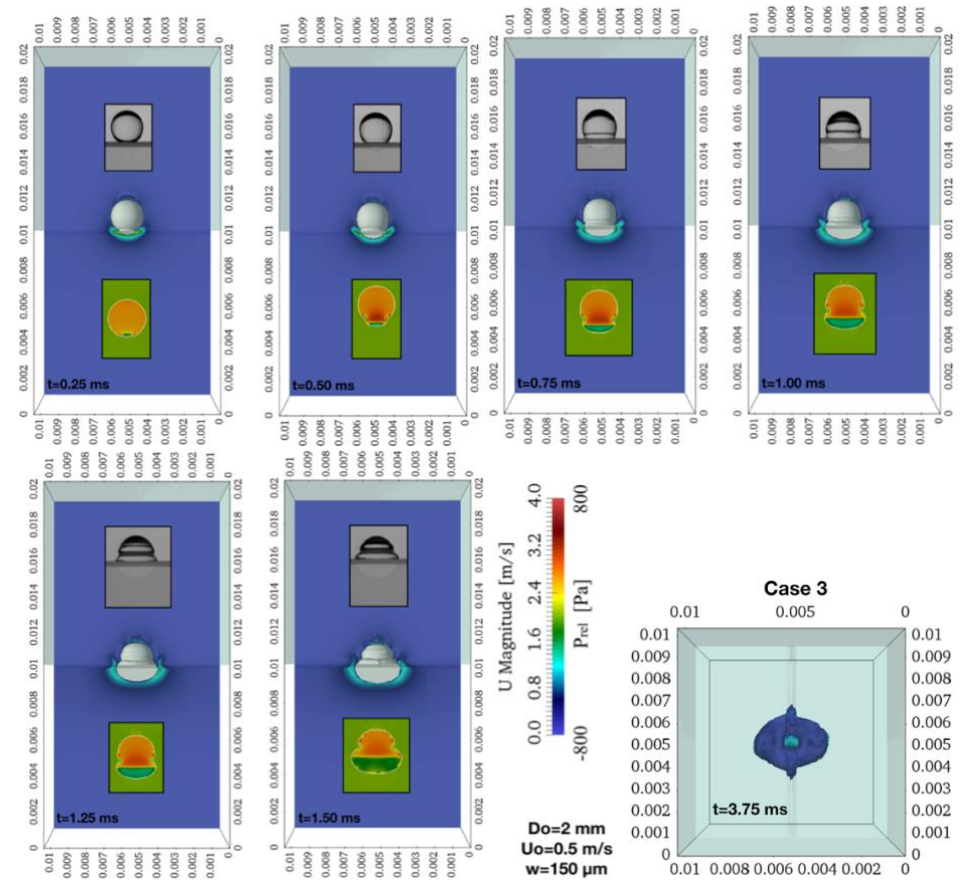

Figure 5. Droplet evolution with time for Case 3 (Table 1). Each time instance up to t = 1.50 ms illustrates the experimental snapshots from [12] (top), the numerically predicted droplet interface with a central section of the predicted velocity distribution (middle/main image) and a central section pressure distribution (bottom). For time t=3.75 ms the top view of the droplet surface is depicted, coloured by the velocity magnitude.

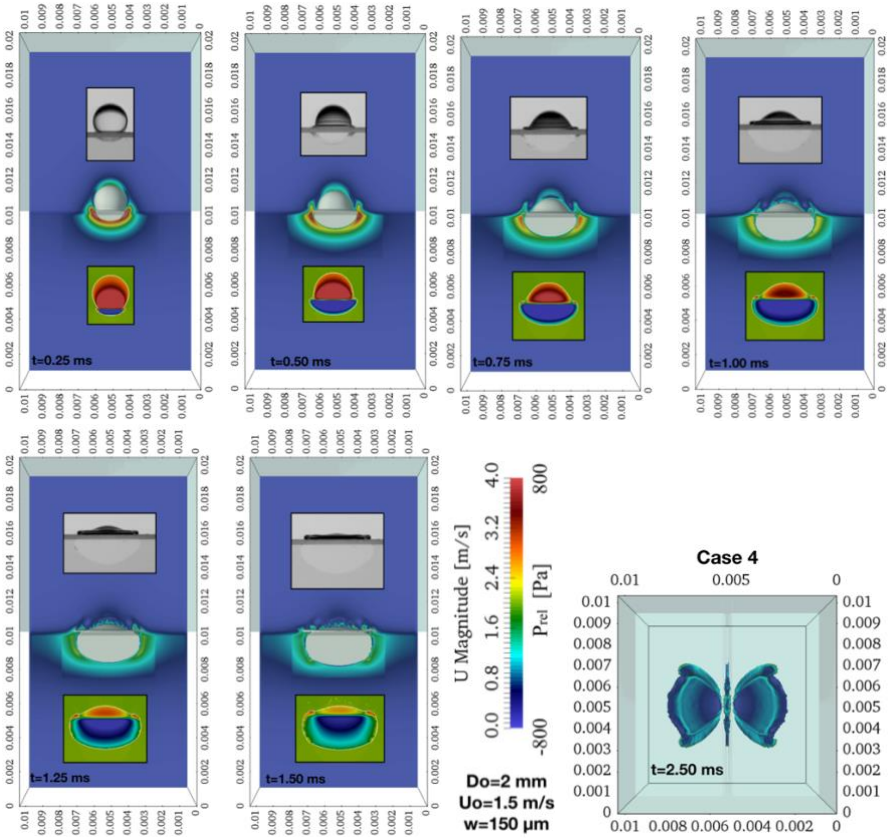

Figure 6. Droplet evolution with time for Case 4 (Table 1). Each time instance up to t = 1.50 ms illustrates the experimental snapshots from [12] (top), the numerically predicted droplet interface with a central section of the predicted velocity distribution (middle/main image) and a central section pressure distribution (bottom). For time t=2.50 ms the top view of the droplet surface is depicted, coloured by the velocity magnitude.

As it can be observed in comparison with experimental snapshots the numerical model predicts quite well the transient evolution of both the horizontal spreading profile of the droplet as well as its imbibition profile within the narrow gap. It is also characteristic that, in agreement with the experimental observations, the droplet remains intact for cases 1 and 3 where the impact velocity is 0.5 m/s but on the contrary it cleaves into two halves for cases 2 and 4 where the impact velocity is 1.5 m/s. This fact may be related to the significantly higher vertical pressure difference between the spreading and penetrating parts of the droplet for cases 2 and 4 (ΔP_{max} within the droplet of approximately 1600 Pa) in comparison to cases 1 and 3 (ΔP_{max} within the droplet of approximately 600 Pa). The higher vertical pressure gradient in cases 2 and 4 creates a stronger movement of liquid in the vertical direction within the narrow gap than the lateral spreading of the droplet that eventually leads to the cleaving of the droplet into two halves. Therefore, it is evident that the break-up or no break-up output of the droplet impact, depends on the impact velocity and it is independent from the width of the narrow gap. However, in order to identify and quantify the effects of impact velocity and narrow gap width on the phenomenon the dimensionless droplet penetration volume within the narrow gap is plotted against the dimensionless time for all cases, in the diagram of Figure 7. The droplet penetration volume is made dimensionless through division with the initial droplet volume before the impact (V_0) while the time is made dimensionless by multiplying it by the impact velocity and dividing by the initial drop diameter (tU_0/D_0).

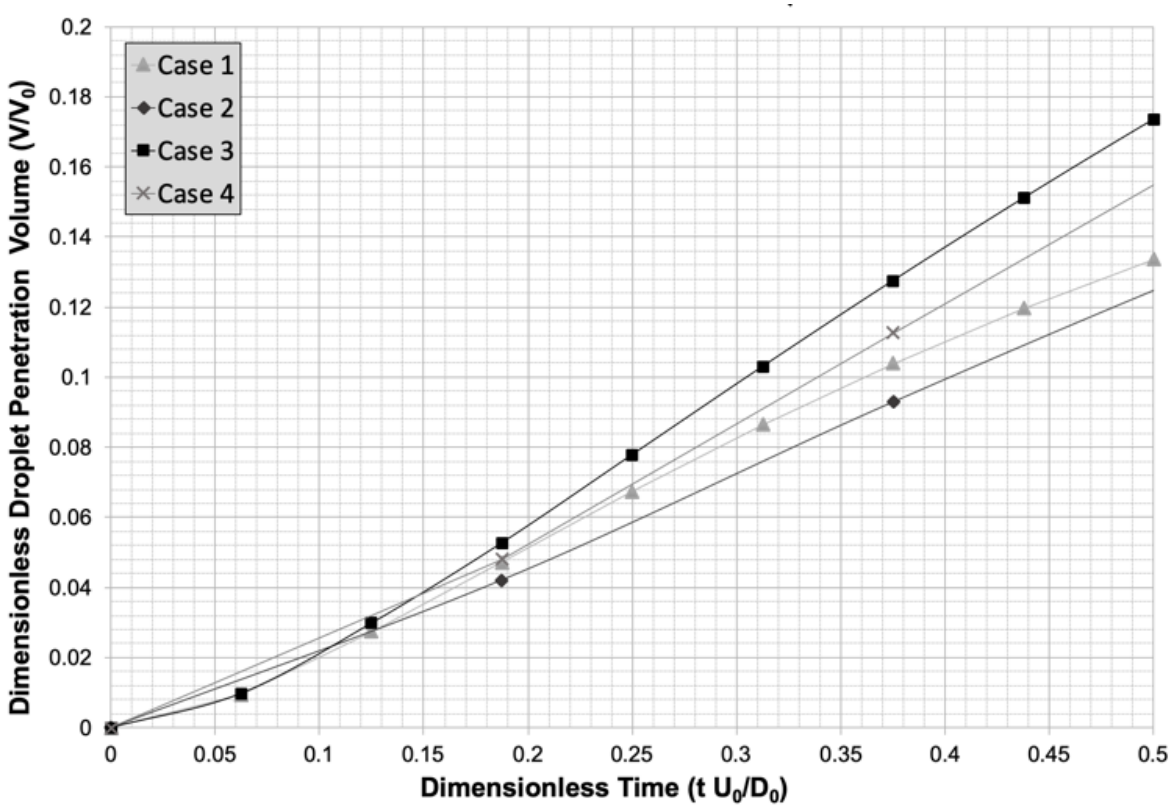

Figure 7. Dimensionless droplet penetration volume with dimensionless time.

As it can be observed comparing cases 1 and 2 or cases 3 and 4 together, it can be concluded that the impact velocity does not significantly affect the early stages of the droplet penetration into the considered narrow gaps, while comparing cases 1 and 3 or cases 2 and 4 together, it can be concluded that the gap width has a more significant effect in the droplet penetration rate into the narrow gap, even from the early stages of the considered droplet impacts.

Conclusions

In the present investigation a series of high resolution, 3D, transient numerical simulations are performed, utilising an enhanced VOF-based CFD model, in order to reproduce specific experimental cases of droplets impacting on narrow gaps, aiming partially to further validate the proposed numerical simulation framework but mainly to understand, identify and quantify the mechanism that governs the potential droplet break-up/cleaving into two subsequent droplets during the droplet spreading phase that was observed in the corresponding experimental investigation. It is shown that the numerical predictions are in very good qualitative agreement with the experimental measurements. Furthermore, the numerical results reveal that the droplet penetration within the narrow gap is governed by the vertical pressure gradients that are developed within the droplet as it simultaneously spreads radically in the horizontal direction and penetrates within the slit in the vertical direction. These vertically developed pressure gradients are a combination of the impact pressure and the capillary pressure. A quantitative comparison of the droplet penetration rates revealed that the impact velocity does not significantly affect the early stages of the droplet penetration into the narrow gap while the gap width has a more significant effect. Finally, from the overall presentation and analysis of the results it is obvious that the proposed enhanced VOF framework can be safely used to further examine the effects of a variety of important controlling parameters to the post-impact characteristics of droplets impinging on porous surfaces. However, a detailed quantitative comparison with the considered experimental runs, needs to be performed in the future.

Acknowledgements

Dr. Andredaki, Dr. Georgoulas and Prof. Marengo would like to acknowledge the usage of the High Performance Computing cluster of the School of Computing Engineering and Mathematics in University of Brighton, the UK's Engineering and Physical Science Research Council support through the grant EP/P013112/1 as well as the financial support from the ESA MAP Projects INWIP and ENCOM 3.

References

[1] Gambaryan-Roisman, T., 2014, “Liquids on Porous Layers: Wetting, Imbibition and Transport Processes,” Curr. Opin. Colloid Interface Sci., **19**(4), pp. 320–335.

[2] Šikalo, Š., Wilhelm, H.-D., Roisman, I. V., Jakirlić, S., and Tropea, C., 2005, “Dynamic Contact Angle of Spreading Droplets: Experiments and Simulations,” Phys. Fluids, **17**(6), p. 062103.

[3] Yokoi, K., Vadillo, D., Hinch, J., and Hutchings, I., 2009, “Numerical Studies of the Influence of the Dynamic Contact Angle on a Droplet Impacting on a Dry Surface,” Phys. Fluids, **21**(7), p. 072102.

[4] Rioboo, R., Marengo, M., and Tropea, C., 2002, “Time Evolution of Liquid Drop Impact onto Solid, Dry Surfaces,” Exp. Fluids, **33**(1), pp. 112–124.

[5] Lee, J. B., Radu, A. I., Vontobel, P., Derome, D., and Carmeliet, J., 2016, “Absorption of Impinging Water Droplet in Porous Stones,” J. Colloid Interface Sci., **471**, pp. 59–70.

[6] Yarin, A. L., 2005, “Drop Impact Dynamics: Splashing,Spreading,Receding,Bouncing...,” Annu. Rev. Fluid Mech., **38**(1), pp. 159–192.

[7] Hapgood, K. P., Litster, J. D., Biggs, S. R., and Howes, T., 2002, “Drop Penetration into Porous Powder Beds,” J. Colloid Interface Sci., **253**(2), pp. 353–366.

[8] Chandra, S., and Avedisian, C. T., 1992, “Observations of Droplet Impingement on a Ceramic Porous Surface,” Int. J. Heat Mass Transf., **35**(10), pp. 2377–2388.

[9] Lee, J. B., Derome, D., and Carmeliet, J., 2016, “Drop Impact on Natural Porous Stones,” J. Colloid Interface Sci., **469**, pp. 147–156.

[10] Roisman, I. V., Lembach, A., and Tropea, C., 2015, “Drop Splashing Induced by Target Roughness and Porosity: The Size Plays No Role,” Adv. Colloid Interface Sci., **222**, pp. 615–621.

[11] Yamamoto, K., Takezawa, H., and Ogata, S., 2016, “Droplet Impact on Textured Surfaces Composed of Commercial Stainless Razor Blades,” Colloids Surfaces A Physicochem. Eng. Asp., **506**, pp. 363–370.

[12] Bouchard, J., and Chandra, S., 2018, “Water Droplet Impact And Spreading On A Narrow Gap,” *Proceedings of The Canadian Society for Mechanical Engineering International Congress 2018, May 27-30*, Toronto, Canada.

[13] Georgoulas, A., Koukouvinis, P., Gavaises, M., and Marengo, M., 2015, “Numerical Investigation of Quasi-Static Bubble Growth and Detachment from Submerged Orifices in Isothermal Liquid Pools: The Effect of Varying Fluid Properties and Gravity Levels,” Int. J. Multiph. Flow, **74**, pp. 59–78.

[14] Vontas, K., Andredaki, M., Georgoulas, A., Nikas, K. S., and Marengo, M., 2017, “Numerical Investigation of Droplet Impact on Smooth Surfaces with Different Wettability Characteristics: Implementation of a Dynamic Contact Angle Treatment in OpenFOAM,” *28th European Conference on Liquid Atomization and Spray Systems*, Polytechnic University of Valencia, ed., Valencia, Spain.

[15] Kistler, S., 1993, “Hydrodynamics of Wetting,” Wettability, **6**, pp. 311–430.

[16] Brackbill, J. ., Kothe, D. ., and Zemach, C., 1992, “A Continuum Method for Modeling Surface Tension,” J. Comput. Phys., **100**(2), pp. 335–354.